

Contents:

Box 1. Single-molecule methods to track the movement of single molecules in the plasma membrane of living cells	----- 2
Box 2. Early times in the development of single-molecule techniques for live cell studies.	----- 4
Box 3. Temporal issues regarding the data acquisition protocol of the camera used for the observation of hop diffusion of membrane molecules in the plasma membrane	----- 8
Box 4. Several concerns regarding the high-speed SPT data of DOPE diffusion	----- 10
Box 5. Algorithm for compartment detection from single-molecule (particle) trajectories.	----- 14
Box 6. Algorithm for the evaluations of various parameters from hop-diffusion trajectories.	-----16
Box 7. Evidence supporting the membrane-skeleton fence and anchored transmembrane-protein picket models for compartmentalization of the cell membrane	----- 17
Box 8. Developmental formation of a diffusion barrier in the neuronal initial segment cell membrane	----- 22
Supplementary on-line TABLE 1 Diffusion coefficients for lipids and GPI-anchored proteins (GPI-AP) in artificial and cell membranes.	----- 28
References for Supplemental Material	----- 30

Box 1. Single-molecule methods to track the movement of single molecules in the plasma membrane of living cells

For direct observations of the movement, localization, and assembly of single membrane molecules, including both lipids and proteins in the plasma membrane, the most common methods are single fluorescent molecule video imaging (SFVI) (34, 69, 82) and single-particle tracking (SPT) (43, 75) (see the figure in this box). In SPT, colloidal gold particles of 20 or 40 nm in diameter are conjugated with small numbers of the ligand or the Fab fragment of the antibody IgG, and after binding to the target molecules on the cell surface, their movements are visualized by transmission optical microscopy (13, 15, 40, 42, 45, 78, 81, 86, 100). The images are electronically enhanced using both analogue and digital circuits, and the locations of individual gold particles in each frame are automatically determined (29, 40).

In SFVI, organic fluorescent dyes or the mutants of green fluorescent protein (mGFPs) are used as probes. To observe molecules located in/on the plasma membrane, fluorescence excitation using total internal reflection or oblique-angle illumination is recommended, to avoid the background signal due to autofluorescence from the cytoplasm or the probe molecules in the cytoplasm, although wide-field illumination can be successfully employed (31-33, 79, 80, 82). Since fluorescence microscopes equipped with these illumination accessories are now commercially available, biomedically-oriented researchers can start single-molecule observations without many initial practical and psychological barriers.

The choice of SPT or SFVI, therefore, depends on the aim of the study (43, 66, 89). However, even when gold probes are chosen for a particular study, one has to examine if the gold probes non-specifically interact with membrane molecules, or if they induce clustering of the target molecules, by comparing the diffusion behavior observed by SPT with that by SFVI (43, 66). Therefore, it is always good to wisely combine SPT and SFVI.

In our laboratory, we tend to start with SFVI observations, since they are generally easier than SPT, which requires the preparation of well-behaved gold probes, and then we proceed with the development of gold probes as the necessity for SPT arises.

A bonus for using gold probes for SPT is that it allows the manipulation of single molecules using the optical trap (20, 42, 44, 78, 97). With the employment of the optical trap, researchers can move the gold-particle-conjugated molecules in the living cell membrane at will.

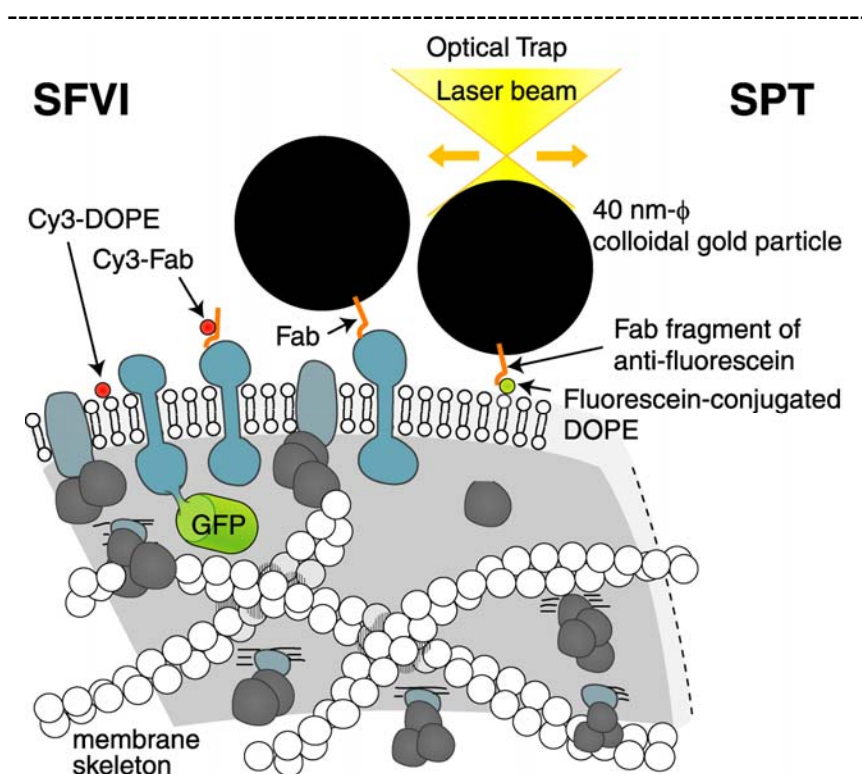


Figure Box 1. Labeling of transmembrane proteins and phospholipids (DOPE) for single-molecule tracking using SPT and SFVI. See the text in this Box for details.

Box 2. Early times in the development of single-molecule techniques for live cell studies.

In principle, even an object smaller than the diffraction limit of light can be visualized by bright-field optical microscopy. The issue here is not the spatial resolution of two points, but the detectability of a single diffracting point. In this case, if the contrast and the signal-to-noise ratio are sufficient, then the presence of the diffracting particle can be detected, and its location (coordinates) can be determined. However, it was surprising for many scientists when de Brabander and his colleagues first showed that colloidal gold particles of 40 nm in diameter could be visualized on the surface of live cells (12, 14, 28). At that time, the detectability was often confused with the spatial resolution, and the visualization of such a small particle was somewhat unexpected. Furthermore, since the cell has various structures that give rise to contrast in the image, until the computer-assisted, real-time (video-rate) contrast enhancement and background subtraction were achieved (1, 35), it was not conceivable that nanometer-sized gold particles could be imaged using optical microscopy. This Belgian group (lead by de Brabander and Geerts) called the method “nanovid microscopy” after “nanometer video-enhanced microscopy” (12), and observed the movement of transferrin receptor and other membrane molecules on the living cell surface in collaboration with Hopkins (13) and Jacobson (15). The smallest gold particle used to study molecular motion on the cell surface was 20 nm in diameter (67), but 5-nm ϕ gold particles can be imaged on a cover slip using bright-field optical transmission microscopy (Sako and Kusumi, unpublished observations).

Gelles et al. (29) and Schnapp et al. (81) were the first to show that the spatial coordinates of submicron particles can be determined with an accuracy at the level of nanometers, which is much smaller than the pixel size of the cameras used to acquire the images. Again, the precision limit is determined by the signal-to-noise ratio of the obtained

image. These results opened the field of tracking molecules in the cell membrane at the level of single or small groups of molecules on the cell surface, which is called “single particle tracking (SPT)”, a term coined by Sheetz (86).

Two independent groups in North Carolina made an early history of SPT. The group lead by Sheetz spearheaded the membrane glycoprotein research, with a special emphasis on integrin-cytoskeletal interactions (23, 41, 51, 62, 77, 85). In addition, they were the first to apply the optical trap, which had been used for motor research in the Sheetz lab, to the membrane research (8, 42, 78, 84), with several projects in collaboration with Edidin (20, 21). The group guided by Jacobson, who initially collaborated with the Belgian group that pioneered the use of gold probes (15), solidified the basis for SPT by studying lipid movement in the cell and artificial membranes and comparing the SPT data with the FRAP results, in addition to studying various mechanisms for retarding the diffusion of membrane molecules in the plasma membrane (15, 47, 48, 76, 87). They were also the first to apply the SPT to raft research (16, 17, 83, 88).

Saxton played a key role in the healthy and robust development of single-molecule tracking in membranes, by providing theoretical input regarding anomalous diffusion and a statistical basis for the analysis and interpretation of single-molecule data, using Monte Carlo simulations (72-75). Kusumi et al. (45) presented a statistical method for the classification of the mode of diffusional motion and an expression that could be used to obtain parameters for molecules undergoing confined diffusion. Based on these methods, the hop diffusion of transmembrane proteins (45, 67) and a phospholipid (24) in the plasma membrane was found.

The problem with SPT lies in the difficulty of differentiating single molecules from small groups of molecules. Statistically, one could compare the SPT data with single fluorescent molecule video imaging (SFVI) data, and evaluate if, or to what extent, the SPT data faithfully reproduce the single-molecule events. However, if one just points to a

moving particle in a video sequence and asks if this particle is bound to one or two molecules, one normally cannot tell. This is the place where SFVI becomes truly useful, in spite of the problems of rapid photobleaching and poor signal-to-noise ratios.

Single fluorescent molecule detection in an aqueous environment was first achieved by Rigler et al. (63) and Nie et al. (57) using confocal laser microscopy, but without imaging. Sase et al. (71), Funatsu et al. (25) and Schmidt et al. (79, 80) were the first to succeed in imaging single fluorescent molecules (still *in vitro*). In particular, Funatsu et al. (25) compared the same image field using both optical and electron microscopy, clearly establishing in scientists' minds that single fluorescent molecules can be imaged in solution, and thus opening the single-molecule era.

Funatsu et al. (25) used total internal reflection fluorescence (TIRF) excitation. TIRF excitation can substantially reduce the background signals of Raman and Rayleigh scattering and fluorescence, because the excitation volume is limited to a layer with a typical thickness of only about 100 nm, on and above the glass surface. However, the original set-up for TIRF excitation was cumbersome for the use of live cells, although it was quite adequate for *in-vitro* studies of single molecules. Tokunaga et al. (96) revived the objective-lens type TIRF excitation, originally proposed by Axelrod (2). Previously, the commercially available fluorescence microscope was a microscope that fluoresces strongly, as K. Kinoshita, Jr. put it, and the objective-lens-type TIRF excitation was simply impractical. When a laser beam was introduced into the microscope, light scattering and fluorescence in the microscope made the imaging of single fluorophores impossible. Tokunaga et al. were the first to take advantage of the great improvements in commercial fluorescence microscopes by the efforts of the manufacturers (possibly inspired by Kinoshita's open criticisms), and Tokunaga et al. further developed this design for practical uses. Given the ease with which live-cell samples can be set up, the simplicity of the optics, the compatibility with micromanipulation and microinjection, and that with normal

epifluorescence and transmission microscopy, the objective lens-type TIRF microscopy has become the choice of many researchers, and a commercial instrument has been available in the market since 2001. The wide-field illumination was also successfully employed by the groups of Schmidt, Schütz, and Moerner (31, 32, 53, 78, 79, 82, 101). They were the first to observe the movement of single fluorescent molecules in artificial membranes (79, 80).

Single fluorescent molecule video imaging (SFVI) in the plasma membrane *in live cells* was first carried out in the research of EGF-receptor activation by Sako et al. (69), and the first imaging of single GFP molecules expressed in live cells was achieved by Iino et al. (34) and Harms et al. ((31); also see Harms et al. (32), but here various GFP mutants were non-specifically attached on the membrane surface). Murakoshi et al. (54) were the first to achieve the imaging of not only location and movement of single molecules, but also the *activation* of single molecules in living cells. In this research, single-molecule fluorescence resonance energy transfer was monitored in live cells in real time, using YFP conjugated to the small G proteins H- or K-Ras as a donor and BodipyTR dye conjugated to GTP as an acceptor. This method may be generally useful for investigations of the activation and dynamics of various G proteins in live cells, at the level of single molecules. The combined use of SPT and SFVI was explored by Fujiwara et al. (24), Nakada et al. (56), and Murase et al. (55).

Box 3. Temporal issues regarding the data acquisition protocol of the camera used for the observation of hop diffusion of membrane molecules in the plasma membrane

A general description of the single-molecule observation methods is given in Box 1. Here, more specific requirements regarding temporal problems for monitoring hop-type movements are summarized, i.e., (1) the frame exposure time (the exposure time for a single frame), (2) the frame acquisition rate, and (3) the total length of tracking a single molecule. In many cameras, the frame exposure time is inverse the frame acquisition rate, but this does not have to be so (and conceptually, they are unconnected). In fact, in recent digital cameras, the frame time can be varied, up to the inverse the frame rate, independently of the frame rate. In the MSD-t plot, the frame (acquisition) rate is reflected as the density of the point. But before we get into these issues, we first emphasize that direct observations of the hops would have been impossible if methods that involved ensemble averaging (like FRAP, where the hop movement of one molecule from a compartment to an adjacent one is smeared out by averaging over all of the molecules under observation) had been employed.

Comparison between Figs. 1a and 1b clearly shows that, in single-molecule tracking, longer frame exposure time of the camera (leading to longer time averaging; item 1 above) or slower frame acquisition rate (i.e., the repetition rate for acquiring the image; at slower rate, the number of the points may be too small to detect the presence of compartments; item 2 above) makes the detection of the hop diffusion impossible. See Fig. 2. The slow frame acquisition rate appears as the insufficient density of the point in the MSD-t plot (every 2 ms vs. every 25 μ s in Fig. 2).

The third point to be considered at the same time is the total observation duration of single molecules, raised as item 3 above. The duration has to be comparable to the

inverse hop rate or the residency time within a compartment to detect the hop events.

Satisfying all of these three requirements is not a simple matter in single fluorescent molecule observations, due to photobleaching of the probe under the high illumination conditions that may be required for accomplishing high-time resolutions (short exposure time for each frame of the camera). Often, the short frame exposure time is first achieved, but then one is often forced to choose either the total length of observation (sacrificing the density of points using time-lapse recording) or the high repetition rate of frame acquisition (sacrificing the total observation period, or depending on one's luck of accidentally obtaining long trajectories). Unless a good compromise between these two could be found, the gradual leveling off of the MSD-t plot may be difficult to detect (judged statistically insignificant), as shown in Fig. 2 right (see 2-ms data).

The rule of thumb in our laboratory is to try to obtain at least 40 points over the average residency time; at a 25- μ s resolution (and the frame rate of 40,000 frames/s), an average hop frequency up to 1 kHz (1-ms residency time) can be observed. This could be achieved by SPT but not single fluorescent molecule methods.

Box 4. Several concerns regarding the high-speed SPT data of DOPE diffusion

In the following, we summarize the concerns and frequently asked questions regarding high-speed SPT data, and try to address these issues.

Q1: What are the major artifacts generated by using colloidal gold probes and how can they be coped with?

A1: a) Non-specific interactions with molecules other than the target molecules. This appears to be under control when well-behaved gold particles were prepared (mostly by varying the conditions of conjugation), because when 60-80% of the extracellular domains of membrane proteins and extracellular matrix proteins were removed, the diffusion of gold-tagged DOPE was not affected. One protocol to be avoided is carrying out prolonged preincubations at low temperatures (like at 4 °C for over 20 min), then washing away the unbound gold particles, and finally observing the gold particles for prolonged periods (over 15 min). If the gold particles that were still attached after all these manipulations were observed, they would certainly be bound to several molecules on the cell surface, which may include molecules other than the target molecule as well as the target molecules (55).

b) Crosslinking by gold probes. This may be the largest problem with gold probes. Murase et al. (55) found that gold probes that were bound on the plasma membrane for periods of less than 150 s (but longer than 3 s, to ensure the binding) exhibited a macroscopic diffusion coefficient (100-ms time window or D_{2-4}) of $0.17 \mu\text{m}^2/\text{s}$ (median), which is comparable to that found for the fluorescently-labeled phospholipid Cy3-DOPE ($0.19 \mu\text{m}^2/\text{s}$), whereas those that stayed longer on the cell surface exhibited a value smaller by a factor of about 3 ($0.066 \mu\text{m}^2/\text{s}$). They estimated that under their experimental conditions, gold particles are bound to monomers (40%), dimers (40%), and greater oligomers (20%). Therefore, for correctly evaluating the macroscopic diffusion coefficient

and the hop frequency of single molecules, and for examining the fidelity of the colloidal gold labeling, SFVI has to be performed for the same molecule in the same cell type, and its results have to be compared with those obtained with SPT. Even if the gold probes induce crosslinking, it would be unlikely to change the observed compartment size significantly. Therefore, the hop rate can be calculated quite accurately by using the macroscopic diffusion coefficient of a fluorescently-labeled molecule (like Cy3-DOPE) and the compartment size determined by SPT with gold-tagged molecules. Furthermore, in optimal cases, like those found in NRK cells, as long as we remain within time windows shorter than 100 ms, the gold-tagged DOPE and Cy3-tagged DOPE exhibited very similar diffusion coefficients (24).

Strategies that can be used for lowering the level of crosslinking include the use of monovalent ligands like Fab (rather than IgG, for the gold particle conjugation), trials of various antibody Fabs until finding the one that gives lowest crosslinking, and simultaneous addition of free ligand that was used to prepare the gold probes (taking advantage of competitive inhibition) when gold particles are added to the cells. In general, one could titrate gold probes, by observing the diffusion coefficient as a function of the variables. Since crosslinking decreases the diffusion coefficient, in general, those that give the largest diffusion coefficient, while retaining the sufficient specific binding ability, are the best choices. The SPT diffusion coefficients always have to be compared with those obtained by SFVI or FRAP, at the early stages of the research of a particular membrane molecule in each cell types used for the study.

Q2: Could the hop movement of gold particles be that from a single membrane molecule to a neighboring molecule?

A2: The hop frequency and the compartment size strongly depend on the cell type (55).

Furthermore, in the same cell type (in all of the four cell types examined thus far; Fujiwara, Iwasawa, and Kusumi, unpublished observations), both DOPE and the

transmembrane protein transferrin receptor sensed the same compartment size. These results argue against the hop movement from one molecule to another.

Q3: Since few researchers have used the CMOS cameras, is it possible that unusual, strange effects by the camera might have been missed?

A3: If this were true, then the same hop events should have been observed even for different cell types and different molecules, which did not happen.

Q4: How could hop diffusion be missed previously? After all, so many people have looked at the diffusion of molecules in the plasma membrane, even at the level of single molecules, and they have not found anything like these results for over 30 years.

A4: See the plot in Fig. 4. In time zones longer than 30 ms, the diffusion appears to be simple Brownian (the slope is very shallow), and this is the time zone explored by previous researchers. Therefore, our results are totally consistent with the results obtained by slower observation methods. We greatly extended the temporal scales to shorter ranges. It is true that the results obtained by SPT have to be corrected by the SFVI results for the crosslinking effect of gold particles. For this argument, see A1 (b) above.

Q5: In the plasma membrane, there are many dips and protrusions, and what appears to be confinement by two-dimensional tracking may represent the time the molecule has to spend to cover the large area of these dips and protrusions. How can we distinguish between the confinement within a compartment and apparent confinement due to dips and protrusions?

A5: In many of the cell types we studied, the difference in the diffusion coefficients between the microscopic and macroscopic diffusion is typically about a factor of 10. To explain this reduction by dips and protrusions, they would have to be very deep (or long), about 100 – 300 nm. In addition, we see confinement basically everywhere in the cell membrane, and thus these dips and protrusions must be everywhere in the membrane. This is refuted by the electron microscopic observations. Remember the electron micrographs

of clathrin coated pits or caveolae ((65), Morone and Kusumi, unpublished observations)?

To explain the retardation of diffusion by dips and protrusions, these electron micrographs would show dips and protrusions greater and deeper than clathrin coated pits and caveolae everywhere in the plasma membrane, and this is totally contrary to the data. Furthermore, thus far, we have always tried to use cell types with small numbers of microvilli and other protrusions, as examined by scanning electron microscopy (in limited cases when we have to use cells with these structures, we observed the surface facing the coverslip, where the plasma membrane appears to have fewer protrusions).

Many other questions have been addressed in related studies, as summarized in Box 7 and the section of “Summary of the evidence supporting the membrane-skeleton fence and anchored transmembrane-protein picket models for compartmentalization of the cell membrane” in the text. Refer to these parts in this review.

Box 5. Algorithm for compartment detection from single-molecule (particle) trajectories.

Compartment detection is performed through the following algorithm. Consider a starting point in the trajectory at frame m , extending over a window of the next n frames. Within this window, the center of geometry of the distribution of the recorded locations is determined, and the maximum radial displacement from this center $R_{MAX}(m, n)$ in this window is determined. This maximum displacement is used to produce an apparent diffusion coefficient for this window of data, through $D_{App}(m, n) \equiv R_{MAX}^2(m, n)/4n\delta t$, where δt is the time differential between consecutive points in the trajectory. For free Brownian diffusion, $D_{App}(m, n)$ is constant (allowing for statistical variations) independent of m or n . If a molecule is temporarily trapped in a finite compartment, then as the window size n increases, $D_{App}(m, n)$ decreases due to the confinement within a compartment. When the window size increases enough to include a hop to an adjacent domain, there is a sharp increase in $D_{App}(m, n)$ due to the extended range of diffusion. By scanning all possible m and n pairs in the full trajectory, a map of $D_{App}(m, n)$ can be produced. Hops are flagged by persistent, sharp increases in $D_{App}(m, n)$ for both a given starting position (e.g. if position m is before a hop and $m+1$ is after a hop, then for all window sizes n , $D_{App}(m, n)$ will be greater than $D_{App}(m+1, n)$) or for the combination of a starting position and a window size (e.g. if the trajectory starting from position m with a window size n , ending at a point $p = m + n$, is wholly within one compartment, and if extending the window size by 1 includes a hop to an adjacent compartment, then $D_{App}(m, n+1)$ will be greater than $D_{App}(m, n)$ for all m and n such that $m + n = p$).

The stochastic nature of diffusion dictates that, at small window sizes, the variation in the apparent diffusion coefficient will be great (even for true Brownian diffusion) and thus it sets limits on the minimum number of points in a compartment required to allow for detection. This will also depend on the noise present in the position detection system. As

such, due caution must be exercised in applying the above algorithm, so as not to choose a plethora of small compartments erroneously. In fact, this algorithm was tested for simple Brownian trajectories generated by Monte Carlo simulations and those for DOPE in liposomes.

Box 6. Algorithm for the evaluations of various parameters from hop-diffusion trajectories.

The analysis of diffusion between finite sized compartments with semi-permeable walls follows from the work of Powles et al. (60). Powles et al. determined the exact solution of the time evolution of the probability distribution due to diffusion through an infinite array of equally spaced, semi-permeable barriers. In their analysis, the time evolution of the probability distribution depends on three parameters: the distance between barriers, L , the true diffusion coefficient in the absence of barriers, D_μ , and the permeability of the barriers, P . They also derived a relationship between the permeability and the long-term diffusion coefficient, D_∞ , $D_\infty/D_\mu = [1 + (PL)^{-1}]^{-1}$, which puts their solution into directly measurable quantities.

The second moment of the probability distribution gives the mean-square displacement ($MSD(t)$) of a particle diffusing through the infinite array of barriers, which is further averaged over all possible starting positions between two barriers. The exact solution of Powles et al. is quite cumbersome, so much so that they even provided a numerical algorithm for determining the time evolution of the probability distribution. Fitting the $MSD(t)$ to experimental data, independently in two orthogonal directions, reveals estimates for the compartment size ($L = (L_x L_y)^{1/2}$, where L_x and L_y are the compartment sizes determined in each direction), the microscopic (short-term) diffusion coefficient within a compartment ($D_\mu = (1/2)(D_{\mu,x} + D_{\mu,y})$, where $D_{\mu,x}$ and $D_{\mu,y}$ are the short-term diffusion coefficients determined in each direction), and the macroscopic (long-term) diffusion coefficient (the rate representing the hop movement over the compartments) ($D_\infty = (1/2)(D_{\infty,x} + D_{\infty,y})$, where $D_{\infty,x}$ and $D_{\infty,y}$ are the long-term diffusion coefficients determined in each direction). The average residency time is determined from the average compartment size, \bar{L} , and the average macroscopic diffusion coefficient, \bar{D}_∞ , as $\tau = \bar{L}^2 / 4\bar{D}_\infty$.

Box 7. Evidence supporting the membrane-skeleton fence and anchored transmembrane-protein picket models for compartmentalization of the cell membrane

The observations that support the models of membrane-skeleton “fence” and transmembrane-protein “pickets” are summarized. Any membrane model has to be compatible with these observations. So far, we have not found any other models that could be consistent with all of these observations: some models could explain one or several of these observations, but not *all* of these observations.

As pointed out in the text, we emphasize the importance of considering all of the data summarized here when new models of the membranes are considered. We are aware of the tendency that one only dwells on the plots based on the relationship between the MSD and the time interval, like those shown in Figs. 2 and 4, trying to make arguments without considering other important data or without careful examination of individual trajectories. In the text, all of the items here are listed, but without explanation. Here, we give more explanation of the data and related models.

- (1) Oligomerization of transmembrane proteins or lipids reduces the macroscopic diffusion coefficient and the intercompartmental hop rate, without affecting the compartment size (oligomerization-induced trapping; (34, 55)). This can be easily explained by the models of fences and pickets, but cannot be naturally explained by the 2-dimensional continuum fluid model, the viscoelastic model for the suppression of membrane molecule diffusion, the general anomalous diffusion model, or the model of long membrane protrusions and deep dips throughout the membrane. In fact, the observations made for oligomers and molecular complexes are those that are almost always neglected by model builders. These are key observations that cannot be understood based on the earlier models, and the new membrane models have to be able to explain or consistent with the greatly suppressed diffusion of oligomers and

molecular complexes. The physiological importance of oligomerization-induced immobilization or slowing of diffusion has already been emphasized in this review.

- (2) The compartment sizes detected by transmembrane proteins (transferrin receptor, α_2 -macroglobulin receptor) and the phospholipid DOPE are the same in all of the cell types examined thus far ((67); Fujiwara, Iwasawa, and Kusumi, unpublished observations, Murase and Kusumi, unpublished observations), suggesting that the membrane skeleton is involved in the hop diffusion of both types of molecules in a relevant way.
- (3) The compartment size detected by the distance of transmembrane proteins being dragged in optical trap experiments employing very weak trapping forces (when the dragged molecule hits an obstacle like the membrane skeleton or transmembrane protein pickets, the force required to drag the molecule suddenly increases, and therefore, by monitoring the force acting on the dragged molecule from the cell, the compartment size can be evaluated) agrees with the compartment size determined by single-molecule diffusion measurements ((68, 70)).
- (4) The optical trapping experiments revealed that the compartment boundaries are elastic, consistent with the model in which the basis for the compartment barrier is the membrane skeleton meshwork ((43, 68, 70, 97); Interactions of transmembrane proteins with the membrane skeleton has been studied by Sheetz group (8, 42, 78, 84) and Edidin et al. (20). These observations cannot be explained by models involving raft-induced compartmentalization of the plasma membrane, crowding of the extracellular surface by the extracellular domain of membrane molecules, anomalous diffusion, or a 2-dimensional continuum fluid. Thus far, we have never found an anomalous diffusion model that could explain such elasticity in the interaction between the diffusant and the obstacles.
- (5) By dragging the membrane skeleton along the plasma membrane, even

transmembrane protein molecules that are not bound to the membrane skeleton could be laterally translocated (97), indicating that the transmembrane protein molecules collide with the membrane skeleton (if the transmembrane protein molecules had not been sensing the presence of the membrane skeleton, then even when the membrane skeleton meshwork was moved, they would not have moved).

- (6) The compartment sizes detected from diffusion measurements of transmembrane proteins and lipids are consistent with the mesh size of the membrane skeleton on the cytoplasmic surface of the plasma membrane, as determined by atomic force microscopy or electron microscope computed tomography ((93, 97), Morone and Kusumi, unpublished observations). The former work was carried out in erythrocyte ghost membranes, and the latter work was done using NRK and FRSK cells with very different compartment sizes (230 and 41 nm, median values). The three-dimensional reconstruction of the membrane skeleton structure was necessary to observe the mesh right on the cytoplasmic surface of the membrane, between 0 and 6 nm from the cytoplasmic surface.
- (7) Monte Carlo simulations reproduced the experimentally observed residency times when only 20-30% of the compartment boundaries were occupied by the anchored transmembrane protein pickets (24, 55, 56). This represents the anchoring of only about 15% of the total transmembrane proteins in the plasma membrane, consistent with the estimate by Bussel et al. (6).
- (8) Hop diffusion of transmembrane proteins and lipids (determined by statistical analyses) depends on the integrity of the membrane skeleton (24, 55, 67, 97). Very mild latrunculin and cytochalasin D treatments increased the compartment size. Note that the effect on the macroscopic diffusion coefficient, under these mild conditions, can be very small, between a factor of 1 and 2, as explained above. Hop diffusion cannot be found in liposomes and in membrane blebs, where the membrane skeleton

is non-existent or largely lost ((24, 55), Suzuki and Kusumi, unpublished observations). In these membranes, the membrane molecules undergo rapid, simple Brownian diffusion that can be characterized by a single diffusion coefficient of 5-10 $\mu\text{m}^2/\text{s}$ for DOPE or 3 $\mu\text{m}^2/\text{s}$ for transmembrane proteins. For an explanation of the lack of the effects of actin depolymerization using FRAP or slow single-molecule tracking occasionally reported recently, see the discussion at the end of the section entitled “The Model of Anchored Transmembrane Protein Pickets, ---”.

- (9) Mild treatments with jasplakinolide, which stabilizes the actin filaments, reduced the macroscopic diffusion coefficient, without strongly affecting the compartment size, by decreasing the hop frequency (24, 55, 56).
- (10) The instances of hops are clearly visible in many cases, and they are detectable with a computer program in the analysis of single-molecule observations with sufficient time resolution ((24, 55), Suzuki and Kusumi, unpublished observations).
- (11) The hop rate of transmembrane proteins increases after the partial removal of the cytoplasmic domain of transmembrane proteins (70, 97).
- (12) The hop diffusion is not affected by removing the major fraction of the extracellular domains of transmembrane proteins and the extracellular matrix ((24, 55), Suzuki and Kusumi, unpublished observations), indicating that these are not the major causes for the induction of hop diffusion. These results also argue against the skepticism with regard to the possible interactions of gold probes with the extracellular domains of transmembrane proteins and the extracellular matrix.
- (13) The removal of cholesterol has no major effects on the hop diffusion ((24, 55), Suzuki and Kusumi, unpublished observations, the hop rate may be decreased slightly, but the classification into the confined + hop diffusion mode was not affected), suggesting that lipid rafts are not the major causes for membrane compartmentalization or hop diffusion.

(14) In hippocampal neurons, the macroscopic diffusion coefficient of DOPE in various regions and developmental stages of the cells correlates well with the concentration of the membrane skeletal proteins, such as ankyrin and actin (see the following section). Furthermore, the level of reduction is non-linearly related to the ankyrin concentration. At the initial stages of ankyrin assembly in the initial segment membrane, the lipid diffusion is hardly affected, but when it reaches a certain threshold level, the DOPE diffusion coefficient suddenly decreases by several hundred-fold. When the correlation between the membrane skeleton and the molecular diffusion in the plasma membrane is discussed or when a plasma membrane model is created, the presence of such a threshold should be considered, with quantitative data.

Box 8. Developmental formation of a diffusion barrier in the neuronal initial segment cell membrane

One of the major functions of the “membrane skeleton fence” and the “anchored-transmembrane protein pickets” may be to form large diffusion barriers in the cell membrane. Recently, Nakada et al. found that neuronal cells develop diffusion barriers in the plasma membrane, using the fence and picket mechanisms (56). The neuron has two distinct domains: one is the somatodendritic domain, which functions in the input of the electrical signal, and the other is the axonal domain, which is responsible for the output of the signal, and each domain has its characteristic membrane proteins. However, the plasma membrane is one continuous membrane, and therefore, there must be a diffusion barrier in the boundary region between the two domains, so the cell can prevent the intermixing of the membrane molecules located in each of these two domains. The domain that separates these two domains is called the initial segment (IS), an elongated domain with a length of $\approx 30 \mu\text{m}$ in mature neurons, located at the foot of the axon.

Previous studies probing the existence of a diffusion barrier in the neuron's IS domain produced contradicting conclusions. There were four landmark papers which addressed the presence of a diffusion barrier in the IS membrane (26, 37, 102, 104). Kobayashi *et al.* first reported the presence of a diffusion barrier in the membrane of the axonal hillock/IS for fluorescently-labeled phospholipids (37), but since they observed the bulk spread of these test molecules incorporated in the entire axonal membrane, Futerman *et al.* argued that most of the incorporated molecules simply did not reach the axonal hillock/IS membrane during the observation period, because the axon is very long (26). Winckler and Poo found that 3,3'-didodecylindocarbocyanine ($\text{diIC}_{12}(3)$) could pass the IS membrane (104). However, the reported diffusion rate of diI in neurites was far greater than those for other diI s or phospholipids (59), suggesting the presence of different diffusion processes (such as intermittent surface diffusion, which cannot be resolved by a

bulk technique like FRAP) due to the short anchoring chains of the diI used (12 carbons versus the normal 16 or 18 carbons). Winckler *et al.*, using laser tweezers, dragged a transmembrane protein (L1) and a GPI-anchored protein (Thy-1) by way of 0.2 $\mu\text{m}\phi$ latex beads bound to these proteins, and found that these molecules were immobilized in the IS membrane due to direct and indirect interactions with f-actin (102, 103). However, since latex beads of this size tend to induce crosslinking of test molecules (44, 64), the results of this dragging experiment may be due to the large sizes of the crosslinked test molecule complexes, and may not reflect the true behaviors of these molecules without crosslinking.

In the study by Nakada *et al.*, the test molecule that they primarily observed was an unsaturated phospholipid, DOPE, which was used in previous studies of membrane compartmentalization and hop diffusion (56). To avoid the ambiguity of bulk observations, they observed the diffusion of individual DOPE molecules using single molecule techniques: SFVI, SPT, and single molecule dragging by laser tweezers. They addressed the following questions: 1) does a diffusion barrier exist in the IS membrane?; 2) if it exists, when is it formed during neuronal development?; and 3) what is the mechanism by which it restricts diffusion? They have established that a diffusion barrier does exist in the IS membrane, determined the stage of neuronal development in which it is formed, and proposed its barrier mechanism.

At 1 day in vitro (DIV), DOPE diffuses rapidly everywhere in the cell membrane, including the IS membrane. In contrast, the diffusion of DOPE in 10-DIV neurons in the IS membrane was severely restricted, whereas it was still free elsewhere on the cell membrane (Fig. Box8-1). Furthermore, colloidal gold probes attached to DOPE in the mature IS membrane could not be dragged laterally by optical tweezers, whereas those attached to the membrane outside the IS or to younger neurons could be dragged freely, suggesting that a diffusion barrier to even phospholipids exists and is formed during neuronal development.

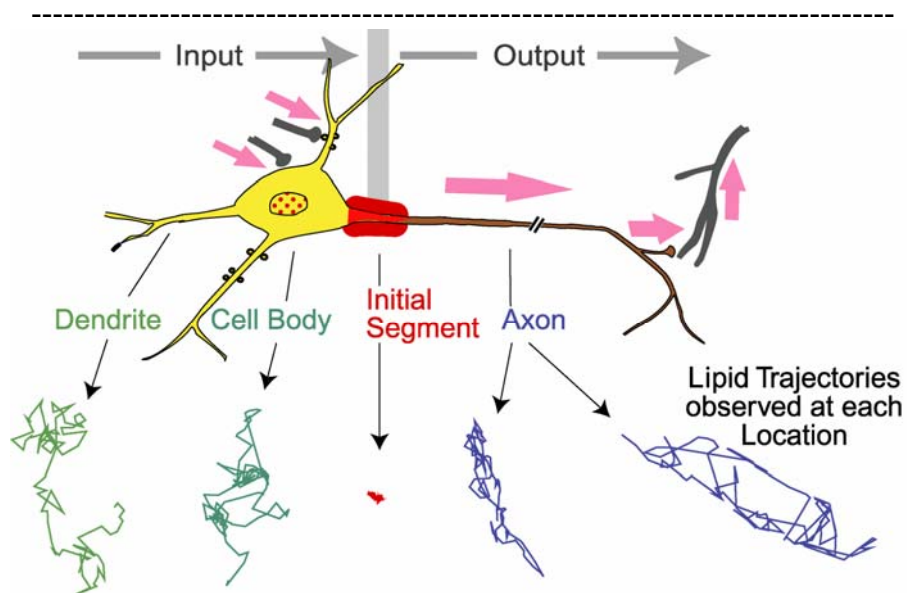


Figure Box 8-1. Neurons develop a diffusion barrier at the initial segment that blocks even lipid diffusion. Polarized distributions of membrane proteins between the somatodendritic domain and the axon are maintained in developed neurons through a diffusion barrier at the region separating the axon from the cell body (IS). Visualization of individual lipid molecules (see the representative trajectories shown in the figure) unequivocally shows that lipid diffusion is restricted at the initial segment.

Nakada et al. examined the mechanism for the barrier formation, following the developmental stages, and found that the immobilization of lipids during development coincides with the accumulation in the IS of Na^+ channels and ankyrin-G (Figs. 9 and 10). Ankyrin-G is known to anchor various transmembrane proteins, including the Na^+ channel, on the membrane skeleton (11, 105) and the accumulation of the Na^+ channel in the IS membrane was also recently reported by other groups (22, 27). These findings, based on the anchored-protein picket model, suggest that the diffusion barrier in the IS membrane may be created by the local concentration of various transmembrane proteins (50) and membrane-skeletal proteins (5, 39), and their binding to each other. Namely, very dense rows of anchored-protein pickets are formed in the IS membrane, and since they are formed over the 30- μm -long domain, they can practically block the macroscopic diffusion

of phospholipids in the IS domain (a rough estimate suggests that it takes over 2 weeks for DOPE to pass this domain). SFVI of the sodium channel confirmed that the channels in the IS region are indeed immobilized in an actin-dependent manner, and that the drug-induced partial actin depolymerization that slightly mobilized the sodium channel greatly increased the DOPE mobility in the IS membrane. In fact, Monte Carlo simulations showed that a sharp decrease in lipid mobility may occur after a small increase in the amount of picket proteins anchored along the membrane skeleton (a decrease by a factor of more than 100 in the diffusion coefficient was induced when the occupancy of picket proteins in the boundary domain was increased from 15 to 25%).

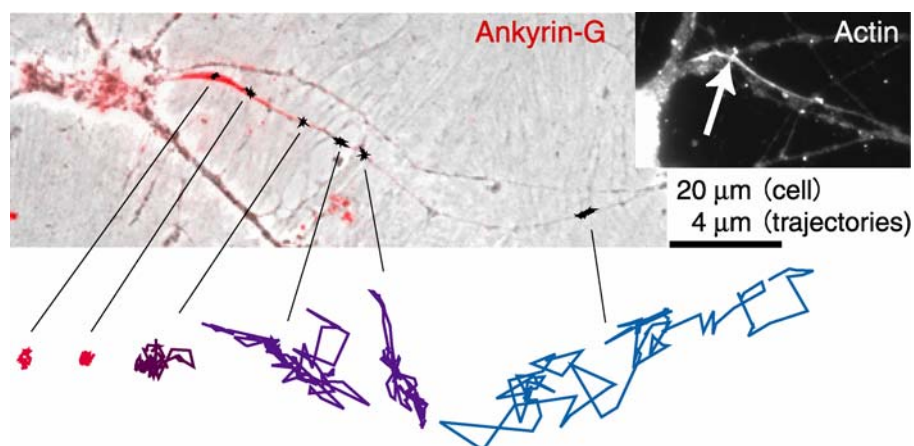


Figure Box 8-2. Lipid diffusion is suppressed where membrane skeletal proteins are concentrated. Lipid movement is suppressed where ankyrin-G is expressed, and the degree of movement suppression correlates well with the level of ankyrin-G expression in the axon of a 10-day old neuron. Immunofluorescence staining with anti-ankyrin-G is shown in red, and the trajectories of gold-labeled DOPE for 3.3 s, recorded at various locations on the axon, are also displayed. (Inset) Actin accumulates in the IS of a 14-DIV neuron, as shown by the sharp, thin, immunofluorescence staining (white arrow). The scale bar shows 20 μm and 4 μm for cell images and trajectories, respectively. The expression level of Nav1.2 (a type of voltage-dependent sodium channel, a transmembrane protein that is anchored to ankyrin-G at its cytoplasmic portion) was also high in the IS (data not shown here).

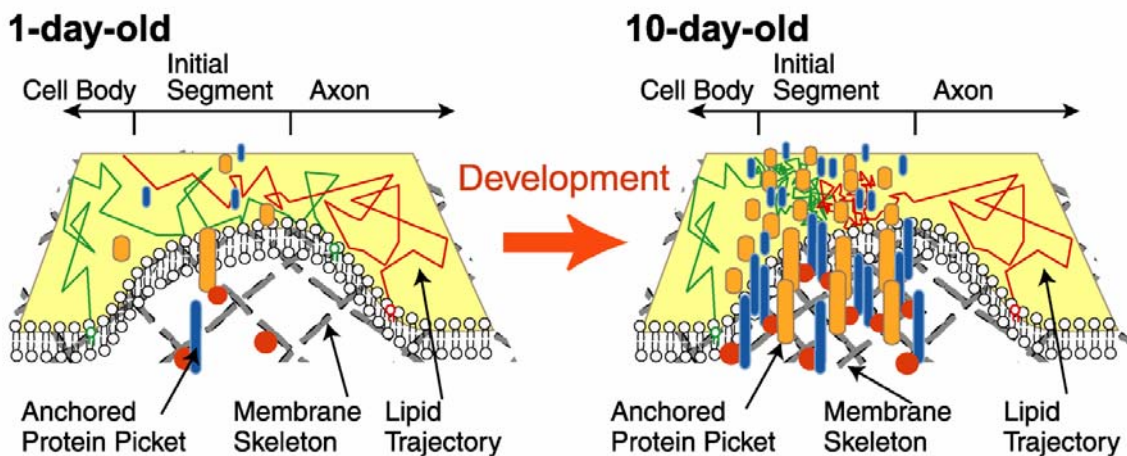


Figure Box 8-3. A schematic model, showing that the increases in the densities of the anchored protein pickets and the membrane skeletal proteins during development form the diffusion barrier in the neuronal IS membrane. Increases in the concentrations of various membrane-skeleton constituent molecules and transmembrane proteins that become immobilized on the membrane skeleton at the initial segment are seen concurrently with the occurrence of the diffusion barrier in the course of neuron maturation by \approx day 11 in vitro. The fence and picket models thus provide a mechanism for the formation of the diffusion barrier in the initial segment membrane, helping the neuron to establish its polarity.

Therefore, the dense rows of various transmembrane protein pickets anchored to and lined up along the actin-based membrane skeleton mesh, which cover the entire IS membrane, practically stop the macroscopic diffusion of even phospholipids across the IS region of the membrane. Such a mechanism for diffusion barrier formation might function in the generation of a variety of other diffusion barriers found in various membranes, where the intermixing of membrane molecules between the membrane domains has to be blocked (Fig. 11). The mother-bud neck region of the budding yeast cell membrane acts as a diffusion barrier to membrane molecules. This barrier may be based on the septin-containing thick cortex underneath the plasma membrane, and may help to maintain the protein composition in the neck region membrane (3, 30, 94). In mammalian spermiogenesis, spermatids acquire distinct domains within each cell, and the boundary

regions between the distinct domains hinder the diffusion of membrane molecules between the neighboring domains (4, 58, 61). The tight junction of epithelial cells is located at the boundary region between the apical and basolateral domains. The analogy between epithelial and neuronal polarity has been discussed (9, 10, 18, 33), but whether the barrier mechanism is the same still remains to be answered (19, 98, 99). Overall, since these macroscopic membrane barriers tend to have a dense membrane skeleton and an enrichment of scaffolding proteins, the membrane-skeleton-based picket-fences may play important roles in the creation of these diffusion barriers. In addition, selective exocytosis-endocytosis is likely to be important for the generation and maintenance of the diffusion barrier and the polarized distribution of membrane molecules (22, 33).

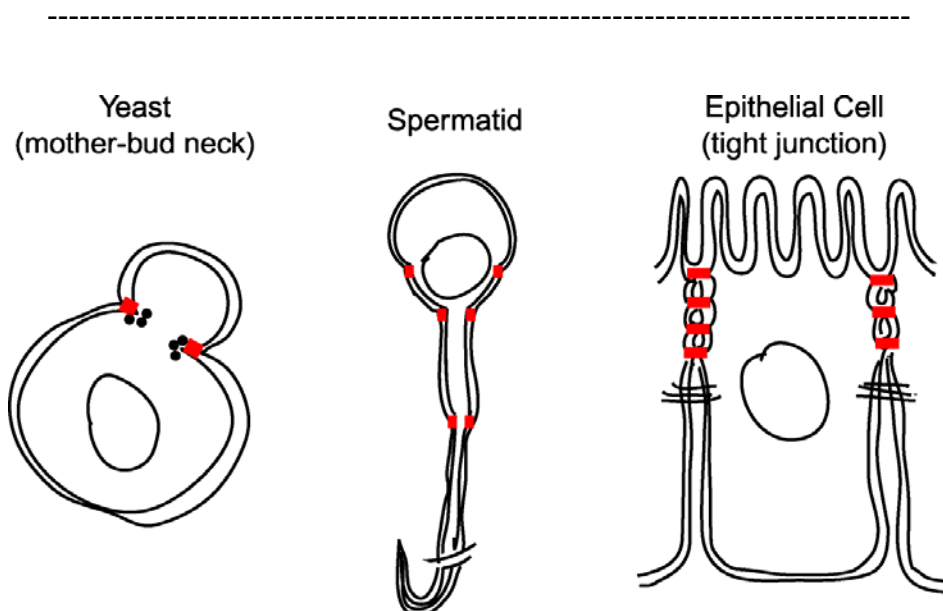


Figure Box 8-4. Various diffusion barriers exist in the continuous fluid membrane, which the membrane-skeleton fence and anchored-protein pickets may help to create. Many cells maintain polarized distributions of membrane molecules in their plasma membranes. The fence and picket models may provide a basic general mechanism for the creation of membrane barriers to maintain the polarized distributions of various membrane molecules.

Supplementary on-line TABLE 1 Diffusion coefficients for lipids and GPI-anchored proteins (GPI-AP) in artificial and cell membranes.

Probe-Lipid (GPI-AP)*	Membrane Type [†]	Method [‡]	Mobile Fraction (%)	Effective D (mean ± SD) ($\mu\text{m}^2/\text{s}$)	Time Window for D (ms)	Temp. ($^{\circ}\text{C}$)	Ref.
ARTIFICIAL MEMBRANES							
TRITC(Cy5)-DPPE	POPE: POPC =7:3	SFD	100	20.6 (± 0.9)	40	23	(91)
EYPC	100% EYPC	NMR	?	5 (± 2)	~100	35	(49)
NBD-DPPE	100% POPC	FRAP	98	13 (± 1.2)	500 [‡]	23	(46)
NBD-PE [#]	100% DMPC	FRAP	~100	7.6 (± 0.3)	2,000 [‡]	30	(7)
NBD-eggPE	EggPC	FRAPP	86	10.5 (± 0.5)	~3,000 [‡]	30	(95)
NBD-eggPE	100% DMPC	FRAPP	?	5 (± 0.3)	~3,000 [‡]	26	(90)
NBD-DMPE	100% DMPC	FRAPP	?	4.3 (± 0.2)	~3,000 [‡]	32	(90)
Gold-DOPE	EggPC: PS: DOPE = 500: 50: 1	SPT	100	9.4 (± 3.7)	100	37	(24)
CELLULAR PLASMA MEMBRANES							
Cy5-DMPE	HASM	SFD	100	0.6 (± 0.04)	12	RT	(82)
Cy3-DOPE	NRK	SFVI	100 [¶]	0.41 (± 0.13) [§]	100	37	(24)
Cy3-DOPE	CHO-B1	SFVI	100 [¶]	0.3 (± 0.23) [§]	100	37	(55)
Cy3-DOPE	T24	SFVI	100 [¶]	0.22 (± 0.14) [§]	100	37	(55)
Cy3-DOPE	FRSK	SFVI	100 [¶]	0.27 (± 0.20) [§]	100	37	(55)
Cy3-DOPE	HEK293	SFVI	100 [¶]	0.41 (± 0.18) [§]	100	37	(55)
Cy3-DOPE	HEPA-OVA	SFVI	100 [¶]	0.37 (± 0.43) [§]	100	37	(55)
Cy3-DOPE	HeLa	SFVI	100 [¶]	0.31 (± 0.31) [§]	100	37	(55)
Cy3-DOPE	Melanocytes	SFVI	100 [¶]	0.40 (± 0.28) [§]	100	37	(55)
Cy3-DOPE	PtK2	SFVI	100 [¶]	0.53 (± 0.30) [§]	100	37	(55)
F18	Bull sperm: acrosome	FRAP	94	2.93 (± 0.15)	~200 [‡]	20	(46)
F18	Bull sperm: principal piece	FRAP	90	1.18 (± 0.26)	~400 [‡]	20	(46)
NBD-PE	Swiss 3T3	FRAP	52	0.34 (± 0.20)	~10,000 ^{**}	18	(52)
NBD-PC [#]	3T3-B	FRAP	54	0.19 (± 0.11)	~10,000 ^{**}	?	(92)
NBD-PC [#]	KMSV-3T3	FRAP	70	0.35 (± 0.23)	~10,000 ^{**}	?	(92)
FITC-DPPE	C3H (lamella)	FRAP	69	0.54 (± 0.27)	~350-700 ^{##}	RT ^{††}	(48)
FITC-DPPE	PtK1 (lamella)	FRAP	71	0.63 (± 0.13)	~350-700 ^{##}	RT ^{††}	(48)
FITC-DPPE	Fish scale fibroblast	FRAP	74	0.95 (± 0.17)	~350-700 ^{##}	RT ^{††}	(48)
YFP-GL-GPI	Cos-7	FRAP	91	0.47 (± 0.07)	7500	37	(36)
GFP-GPI	Cos-7	FRAP	93	0.7	5000	37	(36)
GFP-CD59	Cos-7	FRAP	92	0.6	5800	37	(36)

Modified from Table 1 in Murase et al. (55) with copyright permission.

*TRITC-DPPE, *N*-(6-tetramethylrhodaminethiocarbonyl)-1, 2-dihexadecanoyl-*sn*-glycero-3-phosphoethanolamine; EYPC, egg yolk phosphatidylcholine; NBD, *N*-(4-nitrobenzo-2-oxa-1,3-diazole); DMPE, 1, 2-dimyristoyl-*sn*-glycero-3-phosphoethanolamine; FITC, fluorescein isothiocyanate; DOPE, 1,2-dioleoyl-*sn*-glycero-3-phosphoethanolamine; F18, 5-(*N*-octa-decanoyl)aminofluorescein.

[#]Unknown acyl chains.

[†]POPE, 1-palmitoyl-2-oleoyl-*sn*-glycero-3-phosphoethanolamine; POPC, 1-palmitoyl-

2-oleoyl-*sn*-glycero-3-phosphocholine; DMPC, 1, 2-dimyristoyl-*sn*-glycero-3-phosphocholine; PS, bovine brain phosphatidylserine; NRK, normal rat kidney fibroblasts; HASM, human coronary artery smooth muscle; T24, human carcinoma epithelial cells; FRSK, fetal rat skin keratinocyte; PtK2, rat kangaroo normal kidney; CHO-B1, CHO-K1 cells (Chinese hamster ovary) transfected with murine Fcγ receptor type B1, called CHO-B1 (Miettinen et al., 1989; 1992); HEK293, human embryonic kidney; HEPA-OVA, mouse hepatoma cells; HeLa, Homo sapiens cervix; melanocytes, murine amelanotic melan-c melanocytes; 3T3-B, BALB/c 3T3 fibroblasts; KMSV-3T3, Kirsten murine sarcoma virus-transformed 3T3-B fibroblasts; C3H, mouse embryo fibroblasts; PtK1, rat kangaroo normal kidney.

^{||}SFD, single fluorescence molecule detection (epifluorescence); SFVI, single fluorescence molecule video imaging; NMR, nuclear magnetic resonance; FRAP, fluorescence recovery after photobleaching; FRAPP, fluorescence recovery after pattern photobleaching; SPT, single particle tracking

[¶]Fluctuation (noise) of the coordinates determined for Cy3-DOPE molecules attached on the coverslip (immobile control) gave the nominal diffusion coefficients in the range between 3.0×10^{-4} and $5.9 \times 10^{-3} \mu\text{m}^2/\text{s}$. Meanwhile, all of the fluorescent spots observed in these studies exhibited diffusion coefficients greater than $5.9 \times 10^{-3} \mu\text{m}^2/\text{s}$, and thus it was concluded that the mobile fraction was 100 %.

[§]These SDs include, in addition to the experimental error, the true variations in the diffusion coefficient for individual molecules. The distribution in FRSK cells is given in Murase et al. (55)

^{*}The time required for half of the observed fluorescence recovery to occur, read off from the published recovery curves.

^{||}The half time of the total observation period after pattern photobleaching.

^{**}The time required for half of the observed fluorescence recovery to occur, read off from Koppel (38).

^{###}The time required for half of the observed fluorescence recovery to occur (K. Jacobson, personal communication).

^{††}K. Jacobson, personal communication

References for Supplemental Material

1. Allen RD, Allen NS, Travis JL. 1981. Video-enhanced contrast, differential interference contrast (AVEC-DIC) microscopy: a new method capable of analyzing microtubule-related motility in the reticulopodial network of *Allogromia laticollaris*. *Cell Motil* 1: 291
2. Axelrod D. 1989. Total internal reflection fluorescence microscopy. *Methods Cell Biol* 30: 245
3. Barral Y, Mermall V, Mooseker MS, Snyder M. 2000. Compartmentalization of the cell cortex by septins is required for maintenance of cell polarity in yeast. *Mol Cell* 5: 841
4. Bartles JR. 1995. The spermatid plasma membrane comes of age. *Trends Cell Biol* 5: 400
5. Berghs S, Aggujaro D, Dirkx R, Jr., Maksimova E, Stabach P, et al. 2000. BetaIV spectrin, a new spectrin localized at axon initial segments and nodes of ranvier in the central and peripheral nervous system. *J Cell Biol* 151: 985
6. Bussell SJ, Koch DL, Hammer DA. 1995. Effect of hydrodynamic interactions on the diffusion of integral membrane proteins: diffusion in plasma membranes. *Biophys J* 68: 1836
7. Chang CH, Takeuchi H, Ito T, Machida K, Ohnishi S. 1981. Lateral mobility of erythrocyte membrane proteins studied by the fluorescence photobleaching recovery technique. *J Biochem* 90: 997
8. Choquet D, Felsenfeld DP, Sheetz MP. 1997. Extracellular matrix rigidity causes strengthening of integrin-cytoskeleton linkages. *Cell* 88: 39
9. Colman DR. 1999. Neuronal polarity and the epithelial metaphor. *Neuron* 23: 649
10. Craig AM, Banker G. 1994. Neuronal polarity. *Annu Rev Neurosci* 17: 267
11. Davis JQ, Lambert S, Bennett V. 1996. Molecular composition of the node of Ranvier: identification of ankyrin-binding cell adhesion molecules neurofascin (mucin+/third FNIII domain-) and NrCAM at nodal axon segments. *J Cell Biol* 135: 1355
12. De Brabander M, Geuens G, Nuydens R, Moeremans M, De Mey J. 1985. Probing microtubule-dependent intracellular motility with nanometre particle video ultramicroscopy (nanovid ultramicroscopy). *Cytobios* 43: 273
13. De Brabander M, Nuydens R, Geerts H, Hopkins CR. 1988. Dynamic behavior of the transferrin receptor followed in living epidermoid carcinoma (A431) cells with nanovid microscopy. *Cell Motil Cytoskeleton* 9: 30
14. De Brabander M, Nuydens R, Geuens G, Moeremans M, De Mey J. 1986. The use of submicroscopic gold particles combined with video contrast enhancement as a simple molecular probe for the living cell. *Cell Motil Cytoskeleton* 6: 105
15. De Brabander M, Nuydens R, Ishihara A, Holifield B, Jacobson K, Geerts H. 1991. Lateral diffusion and retrograde movements of individual cell surface components on single motile cells observed with Nanovid microscopy. *J Cell Biol* 112: 111
16. Dietrich C, Bagatolli LA, Volovyk ZN, Thompson NL, Levi M, et al. 2001. Lipid rafts reconstituted in model membranes. *Biophys J* 80: 1417

17. Dietrich C, Yang B, Fujiwara T, Kusumi A, Jacobson K. 2002. Relationship of lipid rafts to transient confinement zones detected by single particle tracking. *Biophys J* 82: 274
18. Dotti CG, Simons K. 1990. Polarized sorting of viral glycoproteins to the axon and dendrites of hippocampal neurons in culture. *Cell* 62: 63
19. Dragsten PR, Blumenthal R, Handler JS. 1981. Membrane asymmetry in epithelia: is the tight junction a barrier to diffusion in the plasma membrane? *Nature* 294: 718
20. Edidin M, Kuo SC, Sheetz MP. 1991. Lateral movements of membrane glycoproteins restricted by dynamic cytoplasmic barriers. *Science* 254: 1379
21. Edidin M, Zuniga MC, Sheetz MP. 1994. Truncation mutants define and locate cytoplasmic barriers to lateral mobility of membrane glycoproteins. *Proc Natl Acad Sci U S A* 91: 3378
22. Fache MP, Moussif A, Fernandes F, Giraud P, Garrido JJ, Dargent B. 2004. Endocytotic elimination and domain-selective tethering constitute a potential mechanism of protein segregation at the axonal initial segment. *J Cell Biol* 166: 571
23. Felsenfeld DP, Choquet D, Sheetz MP. 1996. Ligand binding regulates the directed movement of beta1 integrins on fibroblasts. *Nature* 383: 438
24. Fujiwara T, Ritchie K, Murakoshi H, Jacobson K, Kusumi A. 2002. Phospholipids undergo hop diffusion in compartmentalized cell membrane. *J Cell Biol* 157: 1071
25. Funatsu T, Harada Y, Tokunaga M, Saito K, Yanagida T. 1995. Imaging of single fluorescent molecules and individual ATP turnovers by single myosin molecules in aqueous solution. *Nature* 374: 555
26. Futerman AH, Khanin R, Segel LA. 1993. Lipid diffusion in neurons. *Nature* 362: 119
27. Garrido JJ, Giraud P, Carlier E, Fernandes F, Moussif A, et al. 2003. A targeting motif involved in sodium channel clustering at the axonal initial segment. *Science* 300: 2091
28. Geerts H, De Brabander M, Nuydens R, Geuens S, Moeremans M, et al. 1987. Nanovid tracking: a new automatic method for the study of mobility in living cells based on colloidal gold and video microscopy. *Biophys J* 52: 775
29. Gelles J, Schnapp BJ, Sheetz MP. 1988. Tracking kinesin-driven movements with nanometre-scale precision. *Nature* 331: 450
30. Gladfelter AS, Pringle JR, Lew DJ. 2001. The septin cortex at the yeast mother-bud neck. *Curr Opin Microbiol* 4: 681
31. Harms GS, Cognet L, Lommerse PH, Blab GA, Kahr H, et al. 2001. Single-molecule imaging of l-type Ca(2+) channels in live cells. *Biophys J* 81: 2639
32. Harms GS, Cognet L, Lommerse PH, Blab GA, Schmidt T. 2001. Autofluorescent proteins in single-molecule research: applications to live cell imaging microscopy. *Biophys J* 80: 2396
33. Horton AC, Ehlers MD. 2003. Neuronal polarity and trafficking. *Neuron* 40: 277
34. Iino R, Koyama I, Kusumi A. 2001. Single molecule imaging of green fluorescent proteins in living cells: E-cadherin forms oligomers on the free cell surface. *Biophys J* 80: 2667
35. Inoue S. 1981. Video image processing greatly enhances contrast, quality, and speed in polarization-based microscopy. *J Cell Biol* 89: 346

36. Kenworthy AK, Nichols BJ, Remmert CL, Hendrix GM, Kumar M, et al. 2004. Dynamics of putative raft-associated proteins at the cell surface. *J Cell Biol* 165: 735
37. Kobayashi T, Storrie B, Simons K, Dotti CG. 1992. A functional barrier to movement of lipids in polarized neurons. *Nature* 359: 647
38. Koppel DE. 1979. Fluorescence redistribution after photobleaching. A new multipoint analysis of membrane translational dynamics. *Biophys J* 28: 281
39. Kordeli E, Lambert S, Bennett V. 1995. AnkyrinG. A new ankyrin gene with neural-specific isoforms localized at the axonal initial segment and node of Ranvier. *J Biol Chem* 270: 2352
40. Kucik DF, Elson EL, Sheetz MP. 1989. Forward transport of glycoproteins on leading lamellipodia in locomoting cells. *Nature* 340: 315
41. Kucik DF, Kuo SC, Elson EL, Sheetz MP. 1991. Preferential attachment of membrane glycoproteins to the cytoskeleton at the leading edge of lamella. *J Cell Biol* 114: 1029
42. Kuo SC, Sheetz MP. 1992. Optical tweezers in cell biology. *Trends Cell Biol* 2: 116
43. Kusumi A, Sako Y. 1996. Cell surface organization by the membrane skeleton. *Curr Opin Cell Biol* 8: 566
44. Kusumi A, Sako Y, Fujiwara T, Tomishige M. 1998. Application of laser tweezers to studies of the fences and tethers of the membrane skeleton that regulate the movements of plasma membrane proteins. *Methods Cell Biol* 55: 173
45. Kusumi A, Sako Y, Yamamoto M. 1993. Confined lateral diffusion of membrane receptors as studied by single particle tracking (nanovid microscopy). Effects of calcium-induced differentiation in cultured epithelial cells. *Biophys J* 65: 2021
46. Ladha S, Mackie AR, Harvey LJ, Clark DC, Lea EJ, et al. 1996. Lateral diffusion in planar lipid bilayers: a fluorescence recovery after photobleaching investigation of its modulation by lipid composition, cholesterol, or alamethicin content and divalent cations. *Biophys J* 71: 1364
47. Lee GM, Ishihara A, Jacobson KA. 1991. Direct observation of brownian motion of lipids in a membrane. *Proc Natl Acad Sci U S A* 88: 6274
48. Lee GM, Zhang F, Ishihara A, McNeil CL, Jacobson KA. 1993. Unconfined lateral diffusion and an estimate of pericellular matrix viscosity revealed by measuring the mobility of gold-tagged lipids. *J Cell Biol* 120: 25
49. Lindblom G, Johansson LB, Arvidson G. 1981. Effect of cholesterol in membranes. Pulsed nuclear magnetic resonance measurements of lipid lateral diffusion. *Biochemistry* 20: 2204
50. Matsumoto E, Rosenbluth J. 1985. Plasma membrane structure at the axon hillock, initial segment and cell body of frog dorsal root ganglion cells. *J Neurocytol* 14: 731
51. Mecham RP, Whitehouse L, Hay M, Hinek A, Sheetz MP. 1991. Ligand affinity of the 67-kD elastin/laminin binding protein is modulated by the protein's lectin domain: visualization of elastin/laminin-receptor complexes with gold-tagged ligands. *J Cell Biol* 113: 187
52. Metcalf TN, 3rd, Villanueva MA, Schindler M, Wang JL. 1986. Monoclonal antibodies directed against protoplasts of soybean cells: analysis of the lateral mobility of plasma membrane-bound antibody MVS-1. *J Cell Biol* 102: 1350

53. Moerner WE, Fromm DP. 2003. Methods of single-molecule fluorescence spectroscopy and microscopy. *Review of Scientific Instruments* 74: 3597
54. Murakoshi H, Iino R, Kobayashi T, Fujiwara T, Ohshima C, et al. 2004. Single-molecule imaging analysis of Ras activation in living cells. *Proc Natl Acad Sci USA* 101: 7317
55. Murase K, Fujiwara T, Umemura Y, Suzuki K, Iino R, et al. 2004. Ultrafine membrane compartments for molecular diffusion as revealed by single molecule techniques. *Biophys J* 86: 4075
56. Nakada C, Ritchie K, Oba Y, Nakamura M, Hotta Y, et al. 2003. Accumulation of anchored proteins forms membrane diffusion barriers during neuronal polarization. *Nat Cell Biol* 5: 626
57. Nie S, Chiu DT, Zare RN. 1994. Probing individual molecules with confocal fluorescence microscopy. *Science* 266: 1018
58. Olson GE, Winfrey VP, Westbrook VA, Melner MH. 1998. Targeting of the domain-specific integral membrane protein PM52 to the periacrosomal plasma membrane during guinea pig spermiogenesis. *Mol Reprod Dev* 50: 103
59. Popov S, Brown A, Poo MM. 1993. Forward plasma membrane flow in growing nerve processes. *Science* 259: 244
60. Powles GJ, Mallett MJD, Rickayzen G, Evans WAB. 1992. Exact analytic solutions for diffusion impeded by an infinite array of partially permeable barriers. *Proc. R. Soc. Lond. A* 436: 391
61. Primakoff P, Myles DG. 1983. A map of the guinea pig sperm surface constructed with monoclonal antibodies. *Dev Biol* 98: 417
62. Qian H, Sheetz MP, Elson EL. 1991. Single particle tracking. Analysis of diffusion and flow in two-dimensional systems. *Biophys J* 60: 910
63. Rigler R, Mets U, Widengren J, Kask P. 1993. Fluorescence Correlation Spectroscopy with High Count Rate and Low-Background - Analysis of Translational Diffusion. *European Biophysics Journal with Biophysics Letters* 22: 169
64. Ritchie K, Kusumi A. 2003. Single-particle tracking image microscopy. *Methods Enzymol* 360: 618
65. Rothberg KG, Heuser JE, Donzell WC, Ying YS, Glenney JR, Anderson RG. 1992. Caveolin, a protein component of caveolae membrane coats. *Cell* 68: 673
66. Saffman PG, Delbruck M. 1975. Brownian motion in biological membranes. *Proc Natl Acad Sci USA* 72: 3111
67. Sako Y, Kusumi A. 1994. Compartmentalized structure of the plasma membrane for receptor movements as revealed by a nanometer-level motion analysis. *J Cell Biol* 125: 1251
68. Sako Y, Kusumi A. 1995. Barriers for lateral diffusion of transferrin receptor in the plasma membrane as characterized by receptor dragging by laser tweezers: fence versus tether. *J Cell Biol* 129: 1559
69. Sako Y, Minoghchi S, Yanagida T. 2000. Single-molecule imaging of EGFR signalling on the surface of living cells. *Nat Cell Biol* 2: 168
70. Sako Y, Nagafuchi A, Tsukita S, Takeichi M, Kusumi A. 1998. Cytoplasmic regulation of the movement of E-cadherin on the free cell surface as studied by optical tweezers and single particle tracking: corralling and tethering by the

- membrane skeleton. *J Cell Biol* 140: 1227
71. Sase I, Miyata H, Corrie JE, Craik JS, Kinosita K, Jr. 1995. Real time imaging of single fluorophores on moving actin with an epifluorescence microscope. *Biophys J* 69: 323
 72. Saxton MJ. 1982. Lateral diffusion in an archipelago. Effects of impermeable patches on diffusion in a cell membrane. *Biophys J* 39: 165
 73. Saxton MJ. 1987. Lateral diffusion in an archipelago. The effect of mobile obstacles. *Biophys J* 52: 989
 74. Saxton MJ. 1993. Lateral diffusion in an archipelago. Single-particle diffusion.[comment]. *Biophys J* 64: 1766
 75. Saxton MJ. 1997. Single-particle tracking: the distribution of diffusion coefficients. *Biophys J* 72: 1744
 76. Saxton MJ, Jacobson K. 1997. Single-particle tracking: applications to membrane dynamics. *Annu Rev Biophys Biomol Struct* 26: 373
 77. Schmidt CE, Dai J, Lauffenburger DA, Sheetz MP, Horwitz AF. 1995. Integrin-cytoskeletal interactions in neuronal growth cones. *J Neurosci* 15: 3400
 78. Schmidt CE, Horwitz AF, Lauffenburger DA, Sheetz MP. 1993. Integrin-cytoskeletal interactions in migrating fibroblasts are dynamic, asymmetric, and regulated. *J Cell Biol* 123: 977
 79. Schmidt T, Schutz GJ, Baumgartner W, Gruber HJ, Schindler H. 1995. Characterization of Photophysics and Mobility of Single Molecules in a Fluid Lipid-Membrane. *J Phys Chem* 99: 17662
 80. Schmidt T, Schutz GJ, Baumgartner W, Gruber HJ, Schindler H. 1996. Imaging of single molecule diffusion. *Proc Natl Acad Sci U S A* 93: 2926
 81. Schnapp BJ, Gelles J, Sheetz MP. 1988. Nanometer-scale measurements using video light microscopy. *Cell Motil Cytoskeleton* 10: 47
 82. Schutz GJ, Kada G, Pastushenko VP, Schindler H. 2000. Properties of lipid microdomains in a muscle cell membrane visualized by single molecule microscopy. *Embo J* 19: 892
 83. Sheets ED, Lee GM, Simson R, Jacobson K. 1997. Transient confinement of a glycosylphosphatidylinositol-anchored protein in the plasma membrane. *Biochemistry* 36: 12449
 84. Sheetz MP. 1998. Laser tweezers in cell biology. Introduction. *Methods Cell Biol* 55: xi
 85. Sheetz MP, Baumrind NL, Wayne DB, Pearlman AL. 1990. Concentration of membrane antigens by forward transport and trapping in neuronal growth cones. *Cell* 61: 231
 86. Sheetz MP, Turney S, Qian H, Elson EL. 1989. Nanometre-level analysis demonstrates that lipid flow does not drive membrane glycoprotein movements. *Nature* 340: 284
 87. Simson R, Sheets ED, Jacobson K. 1995. Detection of temporary lateral confinement of membrane proteins using single-particle tracking analysis. *Biophys J* 69: 989
 88. Simson R, Yang B, Moore SE, Doherty P, Walsh FS, Jacobson KA. 1998. Structural mosaicism on the submicron scale in the plasma membrane. *Biophys J* 74: 297

89. Singer SJ, Nicolson GL. 1972. The fluid mosaic model of the structure of cell membranes. *Science* 175: 720
90. Smith LM, Rubenstein JL, Parce JW, McConnell HM. 1980. Lateral diffusion of M-13 coat protein in mixtures of phosphatidylcholine and cholesterol. *Biochemistry* 19: 5907
91. Sonnleitner A, Schutz GJ, Schmidt T. 1999. Free brownian motion of individual lipid molecules in biomembranes. *Biophys J* 77: 2638
92. Swaisgood M, Schindler M. 1989. Lateral diffusion of lectin receptors in fibroblast membranes as a function of cell shape. *Exp Cell Res* 180: 515
93. Takeuchi M, Miyamoto H, Sako Y, Komizu H, Kusumi A. 1998. Structure of the erythrocyte membrane skeleton as observed by atomic force microscopy. *Biophys J* 74: 2171
94. Takizawa PA, DeRisi JL, Wilhelm JE, Vale RD. 2000. Plasma membrane compartmentalization in yeast by messenger RNA transport and a septin diffusion barrier. *Science* 290: 341
95. Tamm LK. 1988. Lateral diffusion and fluorescence microscope studies on a monoclonal antibody specifically bound to supported phospholipid bilayers. *Biochemistry* 27: 1450
96. Tokunaga M, Kitamura K, Saito K, Iwane AH, Yanagida T. 1997. Single molecule imaging of fluorophores and enzymatic reactions achieved by objective-type total internal reflection fluorescence microscopy. *Biochem Biophys Res Commun* 235: 47
97. Tomishige M, Sako Y, Kusumi A. 1998. Regulation mechanism of the lateral diffusion of band 3 in erythrocyte membranes by the membrane skeleton. *J Cell Biol* 142: 989
98. van Meer G, Gumbiner B, Simons K. 1986. The tight junction does not allow lipid molecules to diffuse from one epithelial cell to the next. *Nature* 322: 639
99. van Meer G, Simons K. 1986. The function of tight junctions in maintaining differences in lipid composition between the apical and the basolateral cell surface domains of MDCK cells. *EMBO J* 5: 1455
100. Varma R, Mayor S. 1998. GPI-anchored proteins are organized in submicron domains at the cell surface. *Nature* 394: 798
101. Vrljic M, Nishimura SY, Brasselet S, Moerner WE, McConnell HM. 2002. Translational diffusion of individual class II MHC membrane proteins in cells. *Biophys J* 83: 2681
102. Winckler B, Forscher P, Mellman I. 1999. A diffusion barrier maintains distribution of membrane proteins in polarized neurons. *Nature* 397: 698
103. Winckler B, Mellman I. 1999. Neuronal polarity: controlling the sorting and diffusion of membrane components. *Neuron* 23: 637
104. Winckler B, Poo MM. 1996. No diffusion barrier at axon hillock. *Nature* 379: 213
105. Zhou D, Lambert S, Malen PL, Carpenter S, Boland LM, Bennett V. 1998. AnkyrinG is required for clustering of voltage-gated Na Channels at axon initial segments and for normal Action potential firing. *J. Cell Biol.* 143: 1295